Journal of Physics and Chemistry of Solids 134 (2019) 133–140

Contents lists available at ScienceDirect

Journal of Physics and Chemistry of Solids

journal homepage: www.elsevier.com/locate/jpcs

Biosynthesis of NiO nanoparticles for photodegradation of free cyanide solutions under ultraviolet light

A.K.H. Bashir[a,b,*], L.C. Razanamahandry[a,b], A.C. Nwanya[a,b,c], K. Kaviyarasu[a,b], W. Saban[a,b], H.E.A. Mohamed[a,b], S.K.O. Ntwampe[d,e], F.I. Ezema[a,b,c], M. Maaza[a,b]

[a] UNESCO-UNISA Africa Chair in Nanosciences-Nanotechnology, PO Box 392, Pretoria, South Africa
[b] Nanosciences African Network (NANOAFNET), iThemba LABS-National Research Foundation, PO Box 722, Somerset West, Western Cape Province, South Africa
[c] Department of Physics and Astronomy, University of Nigeria, Nsukka, Nigeria
[d] Bioresource Engineering Research Group (BioERG), Faculty of Applied Science Department of Biotechnology Cape Peninsula University of Technology, P.O. Box 652, Cape Town, 8000, South Africa
[e] Department of Chemical Engineering, Faculty of Engineering and the Built Enviroment, Cape Peninsula University of Technology, P.O.Box 1906, Bellville, 7535, South Africa

ARTICLE INFO

Keywords:
Biosynthesis
Free cyanide
Metal oxide
Photocatalysis

ABSTRACT

In this study, we used an environmentally friendly green method to synthesize NiO nanoparticles (NiO NPs) with an extract from *Persea americana* seeds for use as photocatalysts in the photodegradation of free cyanide (FCN). The characteristics of the NiO NPs were determined by X-ray diffraction (XRD), transmission electron microscopy (TEM), energy dispersive X-ray spectroscopy (EDS), ultraviolet–visible (UV–Vis) analysis, and Fourier transform infrared (FTIR) spectroscopy. The XRD results indicated a cubic-type structure with space group *Fm3m*, No. (225). Morphological analysis conducted using TEM showed that the NiO NPs had rhombohedral and spherical shapes with slight agglomeration. The particle size calculated based on the TEM results was 11 nm. EDS analysis confirmed the elemental constituents of the samples with Ni and O atoms. The phase purity and chemical bonds in NiO were confirmed using FTIR spectroscopy analysis. UV–Vis analysis indicated that the NiO NPs samples exhibited good optical properties with a well-defined peak at 338.9 nm. The energy band gap E_g obtained for NiO NPs based on the optical analyses was 3.75 eV. The NiO NPs performed well as a photocatalyst under UV light during the photodegradation of FCN, where the maximum photocatalytic oxidation efficiency was 84% after irradiation for 30 min. The FCN photodegradation mechanism was elucidated based on the photocatalytic oxidation of compounds by oxygen with semiconductors.

1. Introduction

Metal oxides nanoparticles (NPs) have a wide range of applications because of their unique physical and chemical properties [1–9]. One of the most important applications of these metal oxide NPs is in photocatalysis. The main characteristics of a photocatalytic system are a suitable band gap, large surface area, stability, and reusability [5–7]. Metal oxides NPs such as TiO_2, CeO_2, ZnO, Fe_2O_3 and NiO possess these characteristics and they perform well in the photocatalytic process [10–15].

During the photocatalytic process, depending on the energy gap value, a metal oxide is activated using either ultraviolet (UV) light, visible (Vis) light, or both, and electron–hole pairs (e^-/h^+) are then generated [15]. If the photogenerated pairs (e^-/h^+) do not recombine, they can produce powerful oxidant $OH^{\blacksquare}$ radicals via the oxidation of OH^- anions or O^- radicals via the reduction of O_2 [7]. The radicals and anions can react with pollutant molecules adsorbed on the surface of the photocatalyst to result in their degradation or transformation into harmless products [15,16]. However, the recombination of electron–hole pairs (e^-/h^+) on the surface of a catalyst can decrease or quench the photocatalytic activity. Thus, the recombination of (e^-/h^+) must be prevented to improve the photocatalytic activity, which can be achieved by using a suitable catalyst support to prevent (e^-/h^+) recombination during the photocatalytic process [17,18].

Recently, it was demonstrated NiO NPs have greater potential applications as photocatalysts compared with other metal oxide NPs [17–24]. Moreover, NiO NP is a p-type semiconductor with a wide band gap of 3.6–4 eV [22], and it exhibits good chemical, magnetic, and optical properties, which may make it suitable for industrial applications such as in antiferromagnetic materials [25], electrode materials

* Corresponding author. UNESCO-UNISA Africa Chair in Nanosciences-Nanotechnology, PO Box 392, Pretoria, South Africa.
E-mail address: abashiruwc@gmail.com (A.K.H. Bashir).

https://doi.org/10.1016/j.jpcs.2019.05.048
Received 20 February 2019; Received in revised form 30 May 2019; Accepted 31 May 2019
Available online 06 June 2019

for lithium-ion batteries [26], electrochemical supercapacitors [27], gas sensors adsorbents [28], optical amplifier and tunable lasers [29], photovoltaic devices [30], and electrochromic materials [31,32]. Consequently, several methods have been used to synthesize NiO NPs, such as the sol–gel method [33], microemulsion-assisted sol–gel procedure [34], solvothermal route [35], hydrothermal method [36], thermal decomposition [37], and precipitation method [38], as well as using extracts from plants including *Moringa oleifera* [22], *Tamarix serotina* [39], *Callistemon viminalis* [40], and *Agathosma betulina* [41]. Recently, environmental pollution by toxic elements has become a severe problem for the global community, and thus many efforts have been made to reduce this pollution. Free cyanide (FCN) is a strong toxic component produced in various industrial activities such as gas production, pharmaceutical, mining, electroplating processes, and coal gasification [42,43]. Physicochemical methods, such as chlorination, electrolytic oxidation, and ozonation, as well as biological methods have been applied to remove cyanides [44–48]. In particular, photocatalytic reactions using metal oxides NPs can be employed to treat inorganic compounds and heavy metals at the same time in an oxidation and adsorption process. For instance, the photocatalytic removal of cyanide using illuminated TiO_2 or ZnO NPs was reported previously [49]. The main advantages of this method are its very simple preparation, low cost, and nontoxicity, as well as the ability to change non-biodegradable compounds into biodegradable organic compounds. In the present study, we prepared NiO NPs using a plant extract for the photodegradation of FCN in a photocatalytic waste removal method.

2. Experimental

2.1. Extract preparation

Fresh *Persea americana* fruits were obtained from Somerset Mall, Cape Town, South Africa. Seeds were collected and washed thoroughly using deionized water. Next, 150 g of the seeds were heated at 60 °C in 1 L of deionized water for 24 h until the color of the mixture changed to dark brown. The change in the color of the mixture to dark brown indicated the decomposition of the bioactive elements of the seeds in the deionized water and the final production of the extract. The extract was filtered two times using filter paper (Whatman No. 1) to remove any impurities and the final extract was kept in a refrigerator until further use.

2.2. Synthesis of NiO NPs

Nickel nitrate hexahydrate (Ni $(NO_3)_2.6H_2O$) was purchased from Sigma Aldrich. The NiO NPs were synthesized using 8 g of (Ni $(NO_3)_2.6H_2O$) salt and then dissolved in 100 mL of the *Persea americana* extract, before heating under constant stirring using a magnetic stirrer at 50 °C for 3 h. The resulting precipitate was collected and centrifuged at 4000 rpm, before washing several times with deionized water to remove any residues from the extract, and then drying at 80 °C in a standard oven for 24 h. Finally, the dried powder was subjected to an extra heat treatment in an open-air furnace at 500 °C for 2 h. Fig. 1 shows a flowchart to illustrate the synthesis of the NiO NPs using the extract from *Persea americana* seeds. Recently, *Persea americana* seeds were found to be rich in bioactive constituents [50] that can act as both reducing and capping agents for NPs [51]. Therefore, the biosynthesis of NiO NPs was performed via three chemical reactions with the solvated Ni^{2+} ions and phytochemicals from the *Persea americana* seeds, i.e., with ascorbic and phenolic acids and flavonoids. The altered chemical behavior of ascorbic acid ($C_6H_8O_6$) and nickel nitrate can result in the oxidation of biological compounds, i.e., ascorbic acid to dehydroascorbic acid ($C_6H_7O_6$) via free radicals, followed by electrostatic attraction between the free radicals and precursor cations. The proposed chemical reaction is as follows:

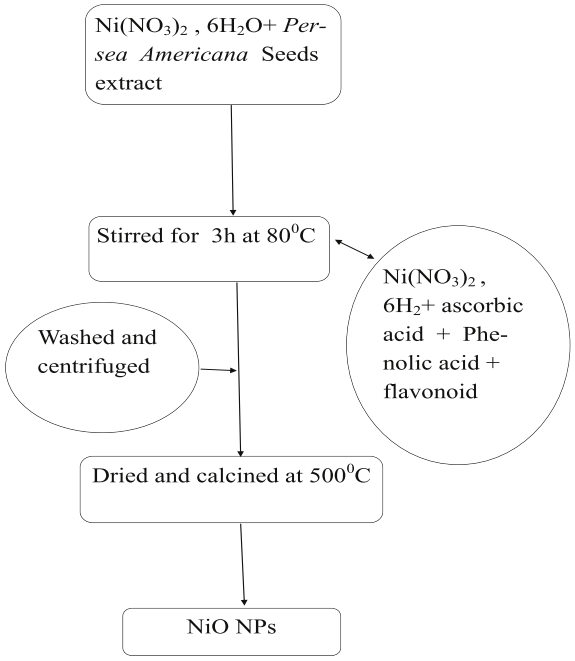

Fig. 1. Flowchart illustrating the synthesis of NiO NPs using the extract obtained from *Persea americana* seeds.

$$Ni(NO_3)_2.6H_2O + 2C_6H_8O_6 \Rightarrow Ni^{2+} + (C_6H_7O_6)_2 + 2NO_2 + 8H_2O \Rightarrow 5000C\ NiO + \text{by-product}$$

2.3. Characterization of NiO NPs

The crystalline structures of the samples was determined by X-ray diffraction (XRD; X-ray diffraction Model Bruker AXS D8 advance) with radiation at λ_{kCuka1} = 1.5406 Å. The morphologies, particle sizes, and size distributions were characterized using high-resolution transmission electron microscopy (TEM) (Philips Technai TEM), where the system operated at an accelerating voltage of 120 kV, and energy dispersive X-ray spectroscopy (EDS) was employed for elemental analysis. UV-VIS-near-infrared analyses were performed with a Nicolette Evolution 100 Spectrometer (Thermo Electron, UK) to analyze the optical properties. Chemical bonds were identified using Fourier transform infrared (FTIR) absorption spectrometry (Shimadzu 8400 s spectrophotometer, 300–4000 cm^1).

2.4. Photocatalytic activity

The photocatalytic performance of NiO (NPs) against FCN solution was determined under UV light (λ_{max} = 365 nm). Before preparing the FCN solution for use in the photocatalytic experiment, we adjusted the pH of the deionized water to 9 in the preparation process to avoid the volatilization of toxic hydrogen cyanide gas (HCN), which is generally produced under acidic conditions. Sodium hydroxide (NaOH) 1 N solution was used to adjust the pH of the deionized water. In the experiment, 0.25 g of potassium cyanide (KCN) powder was dissolved in 100 mL of deionized water in order to obtain an aqueous solution of FCN with a concentration of 1 g L^{-1} (1 g KCN = 0.4 g CN^-). Next, 0.06 g of NiO NP powder was mixed with 100 mL of FCN solution, and the mixture (FCN + NiO NPs) was stirred with a magnetic stirrer in a dark room for 30 min in order complete the adsorption/desorption process for the FCN solution on the surfaces of the NiO NPs. Subsequently, the reaction mixture was exposed to UV light and aliquots of 5 mL were sampled every 10 min during the exposure time of 60 min. The FCN absorption spectrum was then measured using an UV–Vis–near-infrared spectrometer for the 5 mL FCN solutions sampled

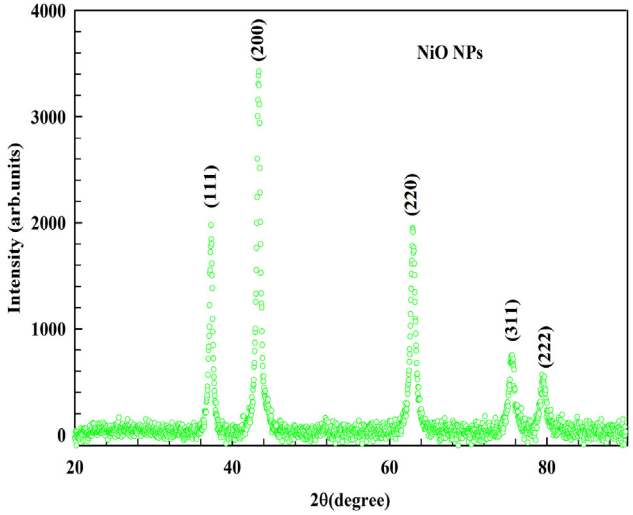

Fig. 2. XRD patterns obtained for NiO NPs prepared with a biosynthesis method using the extract from *Persea americana* seeds.

every 10 min after adding one dose of CN-3 and CN-4 reagents. All of the experiments were conducted in a dark room.

3. Results and discussion

3.1. Crystallography

X-ray diffraction (XRD) analysis was conducted at room temperature using a Bruker Advanced D8 diffractometer to identify the phase purity, composition, particle size, atomic positions, and Wyckoff positions of the NiO NPs sample annealed at 500 °C. The XRD pattern obtained for the annealed NiO NPs (500 °C) is shown in Fig. 2, which confirms the NiO type structure with Bragg peaks centered at 37.249^0, 43.276^0, 62.879^0, 75.416^0, and 79.409^0 corresponding to the 111, 200, 220, 311, and 222 crystalline structures, respectively. All of the Bragg peaks were assigned to the face centered cubic phase with space group *Fm3m* of NiO (JCPDS 1313-99-1) and the lattice constant $a = 4.1771$ Å. No additional peaks were observed in the XRD patterns, thereby indicating the absence of impurity phases in our sample. We used Scherrer's formula to evaluate the crystalline size of the particles in the sample:

$$D = \frac{K\lambda}{\beta cos\theta}, \quad (1)$$

where D is the particle size in Å, K is the shape factor ≃ 0.9, λ is the wavelength (1.5418 Å, CuKα), β is the full width at half maximum of the peak, and θ is the peak position. The crystallite size was estimated at 14.3 nm for the annealed NiO NPs (500 °C) based on the XRD data using Scherer's formula and the FHWM of the intense peak (200).

Rietveld refinement analysis was performed using TOPAS-Academic software to obtain the exact lattice parameter a, unit cell volume V, and atomic positions of the annealed NiO NPs (500 °C), as shown in Fig. 3. The space group setting used for refinement was *Fm3m* for the cubic NaCl-type structure, where O atoms occupied the crystallographic 4a sites and Ni atoms occupied the 4b sites. The resulting cubic crystal structure determined for the annealed NiO NPs (500 °C) is shown in the inset of Fig. 3, and the refined parameters comprising the occupancy and atomic functional positions (Wyckoff positions) are presented in Table 1.

The fitting parameters (R_P as an indicator of the goodness of fit (GOF), R_{wp} as a measure of the GOF calculated point by point and weighted by the standard deviation of the data, and $\chi^2 = R_P/R_{wp}$ (GOF based on statistics)) [52] indicated that the agreement was good between the refined and observed XRD patterns for the cubic NiO NPs

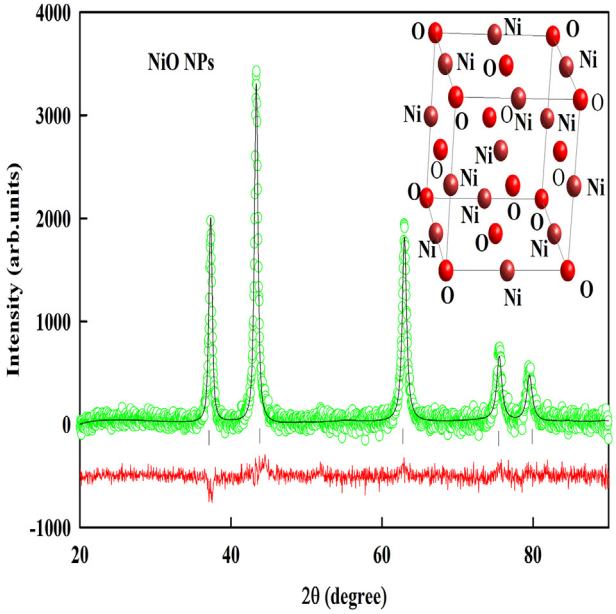

Fig. 3. Rietveld analysis of the XRD patterns obtained for NiO NPs prepared with a biosynthesis method using the extract from *Persea americana* seeds. The observed data are shown by green symbols and the solid black lines represent the results obtained by Rietveld structural refinement. The lower red curves show the difference between the experimental data and the calculated curve, and the vertical black lines are the Bragg positions.

Table 1
Rietveld refined structural parameters obtained for the NiO NPs prepared with a biosynthesis method using the extract from *Persea americana* seeds.

Compound	NiO NPs
Crystal structure	Cubic
Space group	*Fm3m*
Lattice parameters Å	
$a=b=c$	4.17824
$\alpha=\beta=\gamma$	90^0
Unit cell volumeÅ^3	72.9421
Atomic coordinates	
O	
x	0
y	0
z	0
Occupancy	1
Wyckoff site	4a
Ni	
x	0.5
y	0.5
z	0.5
Occupancy	1
Wyckoff position	4b
Refined parameters	
R_p	2.141
R_w	2.763
χ^2	1.179
X-ray density (g/cm^3)	6.78

phase. The lattice parameter and unit cell volume obtained at room temperature by Retrieval refinement for the annealed NiO NPs were $a = 4.178$ Å and $v = 72.942$ Å^3, respectively, which were in good agreement with previously reported data [22].

3.2. FTIR analyses

The FTIR spectrum obtained for the annealed NiO NPs (500 °C) sample is shown in Fig. 4, where the highlighted rectangular areas

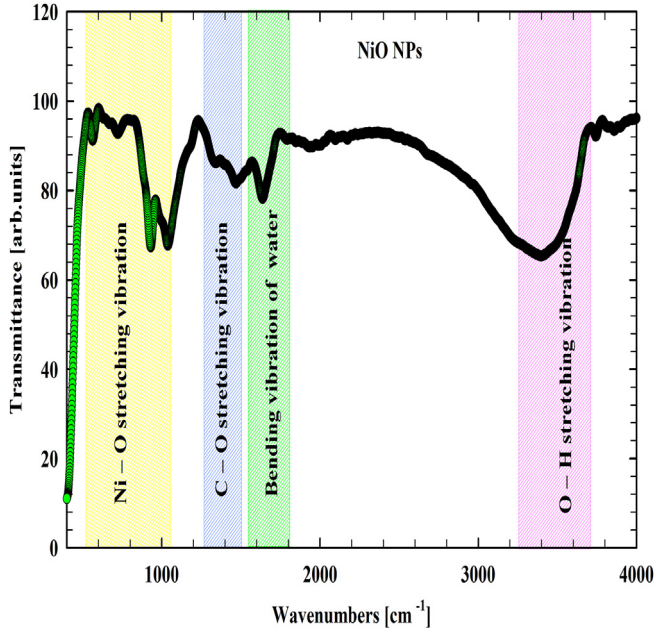

Fig. 4. ATR-FTIR spectrum obtained for the biosynthesized NiO NPs annealed at 500 °C. The highlighted areas indicate the positions of the absorption bands.

indicate that the absorption bands and their positions were highly dependent on the crystalline structure and chemical composition of the NiO NPs. The broad and intense band centered at 3400 cm^{-1} corresponded to the O–H stretching vibration of the interlayer water molecules and the H-bound OH group [54]. The peak observed at 1633 cm^{-1} was assigned to the bending vibration of water molecules [55]. The weak peaks observed at 1433 and 1320 cm^{-1} were assigned to the O–C═O symmetric and asymmetric stretching vibrations and C–O stretching vibration, respectively, which originated from the adsorption of atmospheric CO_2. The lower absorption bands at 918 cm^{-1}, 710 cm^{-1}, and 553 cm^{-1} were assigned to the metal-oxygen stretching frequencies related to Ni–O [22]. In general, the FTIR spectrum confirmed the formation of NiO NPs and it was in good agreement with the results obtained by XRD data, where no impurity phases were detected.

3.3. TEM and EDS analyses

TEM images and the EDS spectrum obtained for the annealed NiO NPs (500 °C) are shown in Fig. 5(a)–(h). The TEM images at different magnifications in Fig. 5(a)–(h) demonstrate the spherical and rhombohedral morphologies of the NiO NPs, which are clearly visible in Fig. 5(d). The irregular shapes of the annealed NiO NP particles were visualized as combinations of spherical and rhombohedral shapes, and the slight agglomeration was ascribed to the magnetic interactions between the particles [22,53]. However, the particle size distribution diagram in Fig. 5(e) shows that the NiO NPs had a small diameter of about 11 nm. The particle size determined from the particle size distribution diagram was very similar to the value of 14.3 nm obtained based on XRD data using Scherrer's formula. The SAED patterns obtained for the NiO NPs are shown in Fig. 5(c), where the lattice fringes are discernible, thereby further demonstrating the polycrystalline nature of the NiO NPs. Moreover, the high resolution TEM image presented in Fig. 4(d) clearly shows that the lattice had an interplanar spacing of about 0.24 nm, which was consistent with the d spacing of (111) for face centered cubic NiO. Finally, the elemental composition of the NiO NPs was determined by analyzing the EDX spectrum, as shown in Fig. 5(e), which verified that the sample mainly comprised Ni and O. The other elements observed in the EDX spectrum, such as C and Cu, were derived from the carbon-coated copper grid used for sample preparation.

3.4. UV analysis

Fig. 6(a) shows the UV–Vis absorption spectroscopy results obtained for the annealed NiO NPs (500 °C) in the range from 200 to 800 nm. Clearly, the NiO NPs exhibited strong absorption in the UV wavelength range (≤400 nm) with a well-defined peak at 338.9 nm. This strong absorption in the UV region was due to the band gap absorption in NiO [56] and this result was in good agreement with data obtained in a previous study [57]. The energy gap was calculated for the annealed NiO NPs (500 °C) using the following equation:

$$(\alpha h\nu)^n = A(h\nu - E_g), \tag{2}$$

where $h\nu$ is the incident photon energy, α is the absorption coefficient, A is a material-dependent constant, E_g is the optical band gap, and n is a constant that depends on the nature of the optical transition [58]. The constant n takes a value of 2 in the case of a direct optical transition and 1/2 for an indirect optical transition. We calculated the direct energy gap for the NiO NPs using $n = 2$ because it gives a good estimation of the band gap value. The direct band gap was estimated from the plot of $(\alpha h\nu)^2$ against $h\nu$, and the band gap energy was then extracted by extrapolating the curve at $\alpha = 0$, as shown in Fig. 6(b). The direct band gap value E_g obtained for the sample was 3.75 eV, which is within the range of (3.6–4 eV) expected for NiO NPs [22].

3.5. Photocatalytic degradation of FCN

The UV–Vis absorption spectrum was obtained at 605 nm for the FCN solution after adding one dose of CN-3 and CN-4 reagents in the presence of the catalyst. Fig. 7 shows the UV spectra recorded every 10 min during the exposure of the FCN solution to the biosynthesized NiO NPs annealed at 500 °C under UV light. When the NiO NPs were used as a photocatalyst under UV light, the maximum absorption wavelength was observed at 605 nm and it gradually decreased, thereby indicating the degradation of the FCN solution in the presence of NiO NPs when irradiated with UV light. The catalytic action depended on the photoresponse of the catalyst by separating the electron–hole pairs. The rates of electron–hole pair splitting and recombination are important indicators of the photocatalytic performance. The FCN degradation process using NiO NPs demonstrated the potential use of this resource as a catalyst, but the process was not successfully completed and it tended to saturate after an irradiation time of 30 min, which could probably be attributed to the recombination of electrons and holes, although this did not totally stop the catalytic process. The degradation efficiency rate with FCN (FCN%) was measured using the following equation:

$$FCN\ \% = \frac{A_0 - A_t}{A_0} \times 100, \tag{3}$$

Where A_0 is the initial absorption of FCN at $t = 0$ and A_t is the absorption of FCN at exposure time t. Fig. 8(a) shows the photocatalytic degradation efficiency with FCN in the presence of NiO NPs. The degradation efficiency with FCN solution was 84% after an irradiation period of 30 min, thereby indicating that the NiO NPs served as a good photocatalyst during the degradation of the FCN solution. This promising result suggests that NiO NPs can be employed as a novel solution for long-term treatment in photocatalytic applications. Thus, long-term photocatalytic tests should be conducted using NiO NPs to confirm their effectiveness as a treatment solution. However, precautions should be taken to protect the NiO NPs from light exposure because their properties will change over time due to the electron-sensitive effects of light sources. According to the photocatalytic oxidation of compounds by oxygen on semiconductors described by Phillips [59], the FCN photodegradation mechanism could be defined as electron–hole (e^-/h^+) separation between the conduction and valence band of the NiO NPs, as

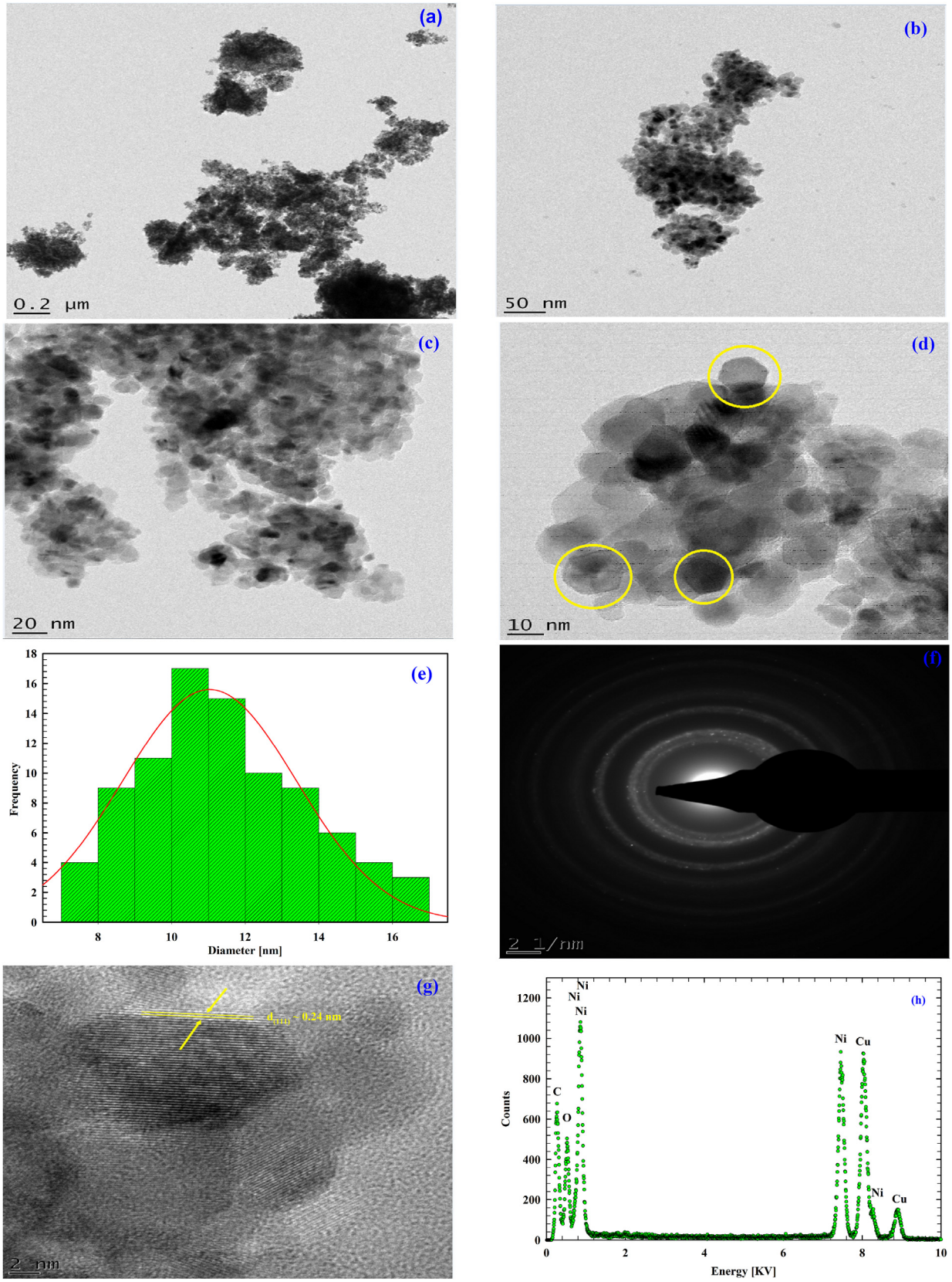

Fig. 5. TEM, high resolution TEM, SAED, and size distribution results for the biosynthesized NiO NPs annealed at 500 °C.

shown in Fig. 8(b). In general, when the surfaces of NiO NPs are illuminated by UV light, the electrons in the valence band become excited and migrate to the conduction band to result in electron–hole separation, which is followed by the diffusion of electron–hole combinations to the surface of the particle, where they interact with water molecules to produce highly reactive species of hydroxide ions OH^- and

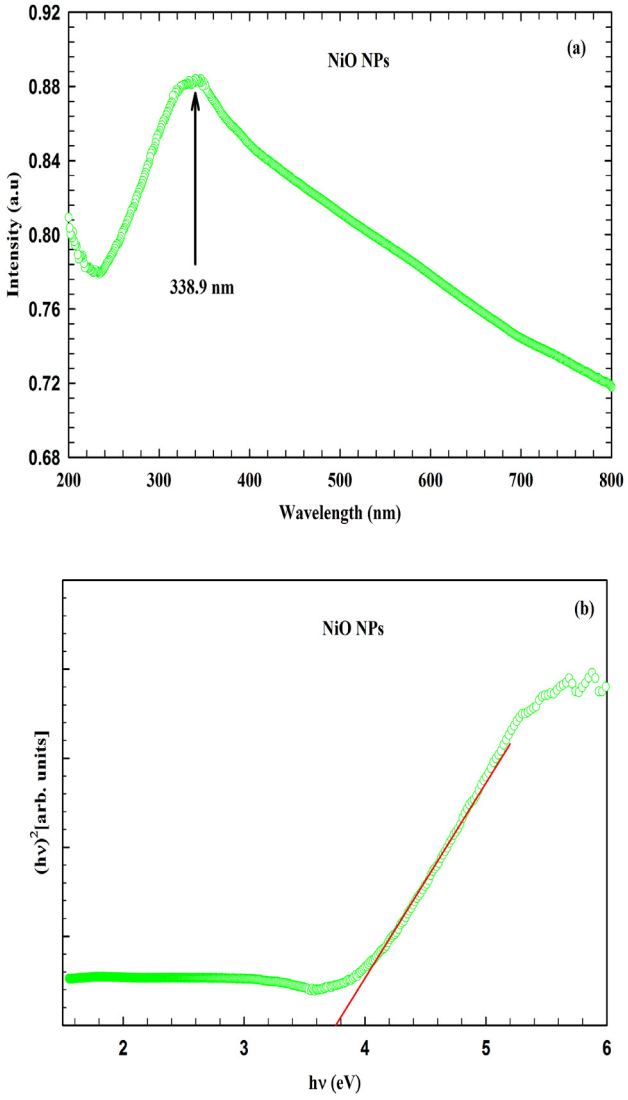

Fig. 6. Optical properties of NiO NPs prepared using the extract from *Persea americana* seeds and annealed at 500 °C: (a) UV–Vis spectrum and (b) band gap energy plot.

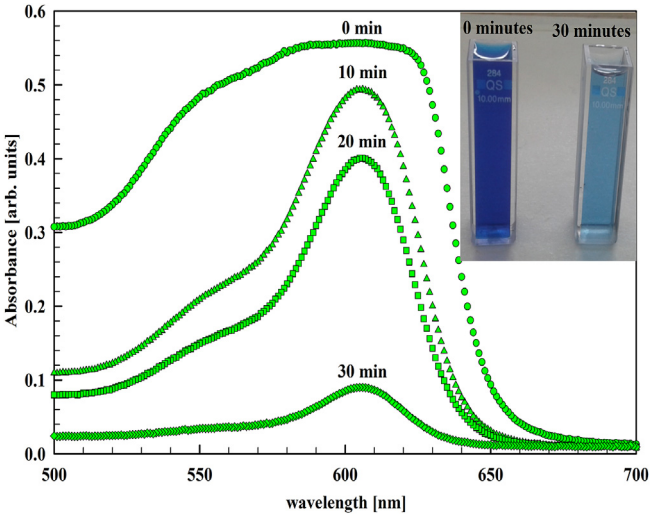

Fig. 7. UV–Vis spectra obtained for FCN with NiO NPs based on samples collected every 10 min during exposure to UV light, where the degradation of FCN occurred on the surfaces of the NiO NPs.

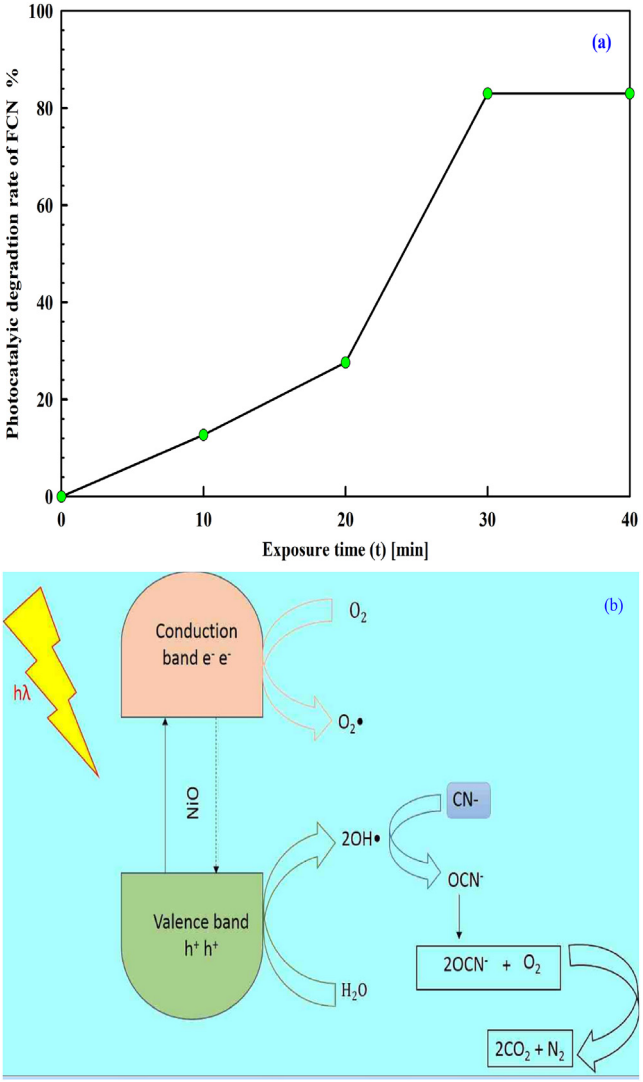

Fig. 8. (a) Degradation rate of FCN on the surfaces of NiO NPs. (b) Degradation mechanism proposed for photo-oxidation of FCN on the surfaces of NiO NPs.

hydroxyl radicals $OH^{\blacksquare}$. In particular, electrons in the conduction band of the NPs react with water molecules to produce hydroxide ions OH^{-}, whereas holes in the valence band interact with water molecules to form hydroxyl radicals ($OH^{\blacksquare}$). The photocatalytic degradation of various organic dyes under light irradiation is generally attributed to their oxidation by reactive oxygen species such as hydroxyl radicals ($OH^{\blacksquare}$). Thus, CN^{-} is oxidized by hydroxyl radicals ($OH^{\blacksquare}$) to form the cyanate anion OCN^{-}, which interacts with oxygen molecules to yield CO_2 and N_2 as the final by-products [60].

$$NiO + h\lambda \rightarrow e^{-} + h^{+} \quad (4)$$

$$2e^{-} + H_2O + \frac{1}{2}O_2 \rightarrow 2OH^{-} \quad (5)$$

$$2h^{+} + 2HO^{-} \rightarrow 2OH^{\blacksquare} \quad (6)$$

$$CN^{-} + 2OH^{\blacksquare} \rightarrow OCN^{-} + H_2O \quad (7)$$

$$2ONC^{-} + O_2 \rightarrow 2CO_2 + N_2 \quad (8)$$

4. Conclusion

In this study, various measurements confirmed the biosynthesis of NiO NPs using the extract from *Persea americana* seeds. TEM analysis

showed that the NiO NPs had rhombohedral and spherical shapes with slight agglomeration. The UV–Vis spectrum showed that the NiO NPs produced a sharp peak at 338.9 nm with a band gap of 3.75 eV. The photocatalytic activity of NiO NPs during the oxidation FCN was good, with a photocatalytic oxidization efficiency of 84% after an irradiation time of 30 min. The NiO NPs biosynthesized using the extract from *Persea americana* seeds had high photocatalytic activity during the degradation of FCN solution, and thus they may be used as a potential candidate for the removal of FCN from wastewater.

Acknowledgement

Support is acknowledged from UNESCO UNISA Africa Chair in Nanosciences/Nanotechnology Laboratories, College of Graduate Studies, University of South Africa, Muckleneuk Ridge, Pretoria, South Africa (Post-Doctoral Fellowship program under contract number: 90396898). We also acknowledge support from the Bioresource Engineering Research Group (BioERG), Faculty of Applied Science Department of Biotechnology, Cape Peninsula University of Technology, Cape Town, South Africa.

Appendix A. Supplementary data

Supplementary data to this article can be found online at https://doi.org/10.1016/j.jpcs.2019.05.048.

References

[1] H. Wang, A.L. Rogach, Hierarchical SnO_2 nanostructures: recent advances in design, synthesis, and applications, Chem. Mater. 26 (2014) 123–133.
[2] K. Kaviyarasu, E. Manikandan, J. Kennedy, M. Jayachandran, R. Ladchumananandasiivam, U. Umbelino De Gomes, M. Maaza, Synthesis and characterization studies of NiO nanorods for enhancing solar cell efficiency using photonupconversion materials, Ceram. Int. 42 (2016) 8385–8394.
[3] K. Anand, C. Tiloke, A. Phulukdaree, B. Ranjan, A. Chuturgoon, S. Singh, R. Gengan, Biosynthesis of palladium nanoparticles by using Moringa oleifera flower extract and their catalytic and biological properties, J. Photochem. Photobiol. B Biol. 165 (2016) 87.
[4] C. Sun, H. Liab, L. Chen, Nanostructured ceria-based materials: synthesis, properties, and applications, Energy Environ. Sci. 5 (2012) 8475–8505.
[5] E. Pelizzetti, C. Minero, Metal oxides as photocatalysts for environmental detoxification, Comments Inorg. Chem. 15 (1994) 297–337.
[6] T. Hisatomi, J. Kubota, K. Domen, Recent advances in semiconductors for photocatalytic and photoelectrochemical water splitting, Chem. Soc. Rev. 43 (2014) 7520–7535.
[7] M.R. Hoffmann, S.T. Martin, W. Choi, D.W. Bahnemann, Environmental applications of semiconductor photocatalysis, Chem. Rev. 95 (1995) 69–96.
[8] A.A. Ezhilarasi, J.J. Vijaya, K. Kaviyarasu, J. Kennedy, R.J. Ramalingam, H.A. Al-Lohedan, Green synthesis of NiO nanoparticles using Aegle marmelos leaf extract for the evaluation of in-vitro cytotoxicity, antibacterial and photocatalytic properties, J. Photochem. Photobiol. B Biol. 180 (2018) 39–50.
[9] K. Anand, K. Kaviyarasu, S. Muniyasamy, S. Mohana Roopan, R.M. Gengan, A.A. Chuturgoon, Bio-Synthesis of silver nanoparticles using agroforestry residue and their catalytic degradation for sustainable waste management, J. Clust. Sci. 28 (2017) 2279–2291.
[10] A. Mobeen Amanulla, S.K. Jasmine Shahina, R. Sundaram, C. Maria Magdalane, K. Kaviyarasu, D. Letsholathebe, S.B. Mohamed, J. Kennedy, M. Maaza, Antibacterial, magnetic, optical and humidity sensor studies of β-$CoMoO_4$-Co_3O_4 nanocomposites and its synthesis and characterization, J. Photochem. Photobiol. B Biol. 183 (2018) 233–241.
[11] T. Prakash, G.V.M. Williams, J. Kennedy, S. Rubanov, Formation of magnetic nanoparticles by low energy dual implantation of Ni and Fe into SiO_2, J. Alloy. Comp. 667 (2016) 255–261.
[12] Y. Subba Reddy, C. Maria Magdalane, K. Kaviyarasu, G. Tessema Mola, J. Kennedy, M. Maaza, Equilibrium and kinetic studies of the adsorption of acid blue 9 and safranin O from aqueous solutions by MgO decked FLG coated Fuller's earth, J. Phys. Chem. Solids 123 (2018) 43–51.
[13] C.M. Magdalane, K. Kaviyarasu, A. Raja, M.V. Arularasu, G.T. Mola, A.B. Isaev, N.A. Al-Dhabi, M.V. Arasu, B. Jeyaraj, J. Kennedy, M. Maaza, Photocatalytic decomposition effect of erbium doped cerium oxide nanostructures driven by visible light irradiation: investigation of cytotoxicity, antibacterial growth inhibition using catalyst, J. Photochem. Photobiol. B Biol. 185 (2018) 275–282.
[14] K. Kasinathan, J. Kennedy, E. Manikandan, M. Henini, M. Maaza, Photodegradation of organic pollutants RhB dye using UV simulated sunlight on ceria based TiO_2 nanomaterials for antibacterial applications, Sci. Rep. 6 (2016) 38064.
[15] K. Kaviyarasu, C. Maria Magdalane, K. Kanimozhi, J. Kennedy, B. Siddhardha, E. Subba Reddy, N. Kumar Rotte, C. Shekhar Sharma, F.T. Thema, D. Letsholathebe, G. Tessema Mola, M. Maaza, Elucidation of photocatalysis, photoluminescence and antibacterial studies of ZnO thin films by spin coating method, J. Photochem. Photobiol. B Biol. 173 (2017) 466–475.
[16] A. Raja, S. Ashokkumar, R.P. Marthandam, J. Jayachandiran, C.P. Khatiwada, K. Kaviyarasu, M. Swaminathan, Eco-friendly preparation of zinc oxide nanoparticles using Tabernaemontana divaricata and its photocatalytic and antimicrobial activity, J. Photochem. Photobiol., B 181 (2018) 53–58.
[17] F. Torki, H. Faghihian, Activity of NiS, NiO and coupled NiS-NiO for degradation of pharmaceutical pollutant cephalexin under visible light, RSC Adv. 7 (2017) 54651–54661.
[18] F. Soofivand, M. Salavati-Niasari, Step synthesis and photocatalytic activity of NiO/graphene nanocomposite under UV and visible light as an effective photocatalyst, J. Photochem. Photobiol. A Chem. 337 (2017) 44–53.
[19] F. Motahari, M.R. Mozdianfard, F. Soofivand, M. Salavati-Niasari, NiO nanostructures: synthesis, characterization and photocatalyst application in dye wastewater treatment, RSC Adv. 4 (2014) 27654–27660.
[20] M. Pirmoradi, S. Hashemian, M.R. Shayesteh, Kinetics and thermodynamics of cyanide removal by ZnO@NiO nanocrystals, Trans. Nonferrous Metals Soc. China 27 (2017) 1394–1403.
[21] P.L. Rajan, J.J. Vijaya, S.K. Jesudoss, K. Kaviyarasu, J. Kennedy, R.J. Ramalingam, H.A. Al-Lohedan, M. Ali Vaali-Mohammed, Green-fuel-mediated synthesis of self-assembled NiO nano-sticks for dual applications-photocatalytic activity on Rose Bengal dye and antimicrobial action on bacterial strains, Mater. Res. Express 4 (2017) 085030.
[22] A.A. Ezhilarasi, J.J. Vijaya, K. Kaviyarasu, M. Maaza, A. Ayeshamariam, L.J. Kennedy, Green synthesis of NiO nanoparticles using Moringa Oleifera extract and their biomedical applications: cytotoxicity effect of nanoparticles against HT-29 cancer cells, J. Photochem. Photobiol. B Biol. 164 (2016) 352–360.
[23] A.F. comănescu, M. Mihaly, A. Meghea, Photocatalytic degradation of organic pollutants using NiO based materials, U.P.B. Sci. Bull., Series B, Chem. Mater. Sci. 74 (2012) 49–60.
[24] E.A. Rogozea, N.L. Olteanu, A.R. Petcu, C.A. Lazar, A. Meghea, M. Mihaly, Extension of optical properties of ZnO/SiO2 materials induced by incorporation of Au or NiO nanoparticles, Opt. Mater. 56 (2016) 45.
[25] S. Krishnakumar, M. Liberati, C. Grazioli, M. Veronese, S. Turchini, P. Luches, S. Valeri, C. Carbone, Magnetic linear dichroism studies of in situ grown NiO thin films, J. Magn. Magn. Mater. 310 (2007) 8–12.
[26] S. Ni, T. Li, X. Yang, X., Fabrication of NiO nanoflakes and its application in lithium ion battery, Mater. Chem. Phys. 132 (2012) 1108–1111.
[27] J. Zhao, H. Liu, Q. Zhang, Preparation of NiO nanoflakes under different calcination temperatures and their supercapacitive and optical properties, Appl. Surf. Sci. 392 (2017) 1097–1106.
[28] Y. Zhang, W. Zeng, New insight into gas sensing performance of nanoneedle-assembled and nanosheet-assembled hierarchical NiO nanoflowers, Mater. Lett. 195 (2017) 217–219.
[29] B. Wu, J.R. Qiu, E. Wu, H. Zeng, Broadband near-infrared luminescence from transparent glass-ceramics containing Ni^{2+}-doped $SrTiO_3$ nanocrystals, Opt. Mater. 35 (2013) 983–987.
[30] M. Borgström, E. Blart, G. Boschloo, E. Mukhtar, A. Hagfeldt, L. Hammarstrm, F. Odobel, Sensitized hole injection of phosphorus porphyrin into NiO: toward new photovoltaic devices, J. Phys. Chem. B 109 (2005) 22928–22934.
[31] X. Wang, L. Wan, T. Yu, J. Zhou, J. Guana, Z. Yu, Z. Li, Z. Zou, Non-basic solution eco-routes to nano-scale NiO with different shapes: synthesis and application, Mater. Chem. Phys. 126 (2011) 494–499.
[32] P.P. Dorneanu, A. Airinei, N. Olaru, M. Homocianu, V. Nica, F. Doroftei, Preparation and characterization of NiO, ZnO and NiO-ZnO composite nanofibers by electrospinning method, Mater. Chem. Phys. 148 (2014) 1029–1035.
[33] S. Sankar, S.K. Sharma, N. An, H. Lee, D.Y. Kima, Y.B. Im, Y.D. Cho, R.S. Ganesh, S. Ponnusamy, P. Raji, L.P. Purohit, Photocatalytic properties of Mn-doped NiO spherical nanoparticles synthesized from sol-gel method, Optik Int. J. Light Electron. Opt. 127 (2016) 10727–10734.
[34] M. Mihaly, A.F. Comanescu, A.E. Rogozea, E. Vasile, A. Meghea, NiO-silica based nanostructured materials obtained by microemulsion assisted sol-gel procedure, Mater. Res. Bull. 46 (2011) 1746–1753.
[35] Z. Qing, L. Haixia, L. Huali, L. Yu, Z. Huayong, L. Tianduo, Solvothermal synthesis and photocatalytic properties of NiO ultrathin nanosheets with porous structure, Appl. Surf. Sci. 328 (2015) 525–530.
[36] K. Motevalli, Z. Zarghami, M. Panahi-Kalamuei, Simple, novel and low-temperature synthesis of rod-Like NiO nanostructure via thermal decomposition route using a new starting reagent and its photocatalytic activity assessment, J. Mater. Sci. Mater. Electron. 27 (2016) 4794–4799.
[37] M.Y. Nassar, H.M. Aly, E.A. Abdelrahman, M.E. Moustafa, Synthesis, characterization, and biological activity of some novel Schiff bases and their Co(II) and Ni(II) complexes: a new route for Co_3O_4 and NiO nanoparticles for photocatalytic degradation of methylene blue dye, J. Mol. Struct. 1143 (2017) 462–471.
[38] L. Gnanasekaran, R. Hemamalini, R. Saravanan, K. Ravichandran, F. Gracia, S. Agarwal, V.K. Gupta, Synthesis and characterization of metal oxides (CeO_2,CuO, NiO, Mn_3O_4, SnO_2 and ZnO) nanoparticles as photo catalysts for degradation of textile dyes, J. Photochem. Photobiol., B 173 (2017) 43–49.
[39] M.A. Nasseri, F. Ahrari, B.A. Zakerinasab, Green Biosynthesis of NiO nanoparticles using aqueous extract of Tamarix serotina and their characterization and application, Appl. Organomet. Chem. 30 (2016) 978–984.
[40] B.T. Sone, X.G. Fuku, M. Maaza, Physical & electrochemical properties of green synthesized bunsenite NiO nanoparticles via Callistemon viminalis' extracts, Int. J. Electrochem. Sci. 11 (2016) 8204–8220.
[41] F.T. Thema, E. Manikandan, A. Gurib-Fakim, M. Maaza, Single phase bunsenite NiO

nanoparticles green synthesis by Agathosma betulina natural extract, J. Alloy. Comp. 657 (2016) 655–661.
[42] J.R. Parga, V. Valenzquez, H.M. Casillas, J.L. Valenzuela, Cyanide detoxification of mining wastewaters with TiO_2 nanoparticles and its recovery by electrocoagulation, Chem. Eng. Tech. 140 (2009) 1901–1908. Ahead of Print:NA.
[43] M. Shirzad Siboni, M.R. Samarghandi, J.K. Yang, S.M. Lee, Photocatalytic removal of cyanide with illuminated TiO_2, Water Sci. Technol. 64 (2011) 1383–1387.
[44] M.A. Barakat, Adsorption behavior of copper and cyanide ions at TiO_2-solution interface, J. Colloid Interface Sci. 291 (2005) 345–352.
[45] M.A. Barakat, Y.T. Chen, C.P. Huang, Removal of toxic cyanide and Cu(II) Ions from water by illuminated TiO_2 catalyst, Appl. Catal. Environ. 53 (2004) 13–20.
[46] P. Jose, D. Xavier, Photocatalytic cyanide oxidation from aqueous copper cyanide solutions over TiO_2 and ZnO, J. Chem. Technol. Biotechnol. 53 (1992) 93–96.
[47] A. Bozzi, I. Guasaquillo, J. Kiwi, Accelerated removal of cyanides from industrial effluents by supported TiO_2photo-catalysts, Appl. Catal. Environ. 51 (2004) 203–211.
[48] L.C. Razanamahandry, H.A. Andrianisa, H. Karoui, K.M. Kouakou, H. Yacouba, Biodegradation of free cyanide by bacterial species isolated from cyanide-contaminated artisanal gold mining catchment area in Burkina Faso, Chemosphere 157 (2016) 71–78.
[49] M. Farrokhi, J. Yang, S. Lee, M. Shirzad-Siboni, Effect of organic matter on cyanide removal by illuminated titanium dioxide or zinc oxide nanoparticles, J. Environ. Health Sci. Eng. 11 (2013) 23.
[50] Y. Ge, X. Si, J. Cao, Z. Zhou, W. Wang, W. Ma, Morphological characteristics, nutritional quality, and bioactive constituents in fruits of two avocado (Persea americana) varieties from Hainan Province, China, J. Agric. Sci. 9 (2017) 2.
[51] A.K.H. Bashir, C.M. Furqan, K. Bharuth-Ram, K. Kaviyarasu, M.B.T. Tchokonte, M. Maaza, Structural, optical and Mössbauer investigation on the biosynthesized α-Fe_2O_3: study on different precursors, Phys. E Low Dimens. Syst. Nanostruct. 111 (2019) 152–157.
[52] M.B.T. Tchokonte, A.K. Bashir, A.M. Strydom, Crystal structure and thermodynamic properties of $NdCu_4Au$ compound, J. Phys. Chem. Solids 90 (2016) 59–64.
[53] X.S. Wang, X. Liu, L. Wen, Y. Zhou, Y. Jiang, Z. Li, Comparison of basic dye crystal violet removal from aqueous solution by low-cost biosorbents, Separ. Sci. Technol. 43 (2008) 3712–3731.
[54] G.J.A.A. Soler-Illia, M. Jobbágy, A.E. Regazzoni, M.A. Blesa, Synthesis of nickel hydroxide by homogeneous alkalinization. Precipitation mechanism, Chem. Mater. 11 (1999) 3140–3146.
[55] Y. Li, X. Xie, J. Liu, M. Cai, J. Rogers, W. Shen, Synthesis of α-$Ni(OH)_2$ with hydrotalcite-like structure: precursor for the formation of NiO and Ni nanomaterials with fibrous shapes, Chem. Eng. J. 136 (2008) 398–408.
[56] X. Wang, J. Song, L. Gao, J. Jin, H. Zheng, Z. Zhang, Optical and electrochemical properties of nanosized NiO via thermal decomposition of nickel oxalate nanofibers, Nanotechnology 16 (2005) 3739.
[57] M. El-Kemary, N. Nagy, I. El-Mehasseb, Nickel oxide nanoparticles: synthesis and spectral studies of interactions with glucose, Mater. Sci. Semicond. Process. 16 (2013) 1747–1752.
[58] R. Branek, H. Kisch, Tuning the optical and photoelectrochemical properties of surface-modified TiO2, Photochem. Photobiol. Sci. 7 (2008) 408.
[59] R. Phillips, Sources and Application of Ultraviolet Radiation, Academic Press, New York, 1983, p. 124.
[60] I.A. Ibrahim, A.A. Ismail, R.M. Mohamed, Degradation of free cyanide by photocatalytic oxidation, Eur. J. Miner. Process. Environ. Prot. 3 (2003) 281–290.